

RESEARCH ARTICLE

Delineating functional segregations of the human middle temporal gyrus with resting-state functional connectivity and coactivation patterns

Jinping Xu^{1,2}  | Hanqing Lyu³ | Tian Li¹ | Ziyun Xu¹ | Xianjun Fu¹ |
Fucang Jia¹ | Jiaojian Wang⁴  | Qingmao Hu¹

¹Institute of Biomedical and Health Engineering, Shenzhen Institutes of Advanced Technology, Chinese Academy of Sciences, Shenzhen, China

²University of Chinese Academy of Sciences, Beijing, China

³Radiology Department, Shenzhen Traditional Chinese Medicine Hospital, Shenzhen, China

⁴Key Laboratory for NeuroInformation of the Ministry of Education, School of Life Science and Technology, University of Electronic Science and Technology of China, Chengdu, China

Correspondence

Qingmao Hu, Institute of Biomedical and Health Engineering, Shenzhen Institutes of Advanced Technology, Chinese Academy of Sciences, Shenzhen 518055, China.
Email: qm.hu@siat.ac.cn

Jiaojian Wang, Key Laboratory for NeuroInformation of the Ministry of Education, School of Life Science and Technology, University of Electronic Science and Technology of China, Chengdu 610054, China.
Email: jiaojianwang@uestc.edu.cn

Funding information

Natural Science Foundation of Guangdong Province, Grant/Award Number: 2017A030313744; Shenzhen Key Basic Research Grant, Grant/Award Numbers: KQJSCX20170731162830878, JCYJ20160331191401141, JCYJ20160531184531506; National Natural Science Foundation of China, Grant/Award Numbers: U1713215, 61671440, 61701078

Abstract

Although the middle temporal gyrus (MTG) has been parcellated into subregions with distinguished anatomical connectivity patterns, whether the structural topography of MTG can inform functional segregations of this area remains largely unknown. Accumulating evidence suggests that the brain's underlying organization and function can be directly and effectively delineated with resting-state functional connectivity (RSFC) by identifying putative functional boundaries between cortical areas. Here, RSFC profiles were used to explore functional segregations of the MTG and defined four subregions from anterior to posterior in two independent datasets, which showed a similar pattern with MTG parcellation scheme obtained using anatomical connectivity. The functional segregations of MTG were further supported by whole brain RSFC, coactivation, and specific RFSC, and coactivation mapping. Furthermore, the fingerprint with predefined 10 networks and functional characterizations of each subregion using meta-analysis also identified functional distinction between subregions. The specific connectivity analysis and functional characterization indicated that the bilateral most anterior subregions mainly participated in social cognition and semantic processing; the ventral middle subregions were involved in social cognition in left hemisphere and auditory processing in right hemisphere; the bilateral ventro-posterior subregions participated in action observation, whereas the left subregion was also involved in semantic processing; both of the dorsal subregions in superior temporal sulcus were involved in language, social cognition, and auditory processing. Taken together, our findings demonstrated MTG sharing similar structural and functional topographies and provide more detailed information about the functional organization of the MTG, which may facilitate future clinical and cognitive research on this area.

KEYWORDS

coactivation connectivity, connectivity-based parcellation, middle temporal gyrus, resting-state functional connectivity

Jinping Xu and Hanqing Lyu authors are contributed equally to this work.

This is an open access article under the terms of the Creative Commons Attribution-NonCommercial License, which permits use, distribution and reproduction in any medium, provided the original work is properly cited and is not used for commercial purposes.

© 2019 The Authors. *Human Brain Mapping* published by Wiley Periodicals, Inc.

1 | INTRODUCTION

Although the middle temporal gyrus (MTG) was traditionally regarded as a cytoarchitecturally homogeneous region (Brodmann, 1909), a large number of studies have demonstrated that it has various functions including language, emotion, memory, and social cognition (Friedman et al., 1998; Giraud et al., 2004; Goel, Gold, Kapur, & Houle, 1998; Hesling, Clement, Bordessoules, & Allard, 2005; McDermott, Petersen, Watson, & Ojemann, 2003; Mirz et al., 1999; Rizzolatti et al., 1996; Sato, Toichi, Uono, & Kochiyama, 2012; Whitney, Jefferies, & Kircher, 2011). Moreover, MTG impairments have been widely reported to be associated with various brain disorders, such as autism spectrum disorder (Assaf et al., 2013; Ogawa et al., 2019), major depression disorders (Cheng et al., 2019; Liu et al., 2019), bipolar disorder (Tian et al., 2019), obsessive-compulsive disorder (Fan et al., 2017), and temporal lobe epilepsy (Bozkurt et al., 2016). And the MTG was an optimal location for surgical treatment for temporal lobe epilepsy, known as trans-MTG approach (Bozkurt et al., 2016; Bujarski et al., 2013; Wheatley, 2008). Given its functional diversity and close relationship with different brain disorders, building a fine-grained functional atlas for MTG is crucial for delineating the functional specialization to guide the clinical accurate neurosurgery and treatment.

In order to explore whether functionally distinctive subregions exist in human MTG, several schemes have been performed to parcellate the MTG into different components based on myeloarchitectonic properties (Sewards, 2011), anatomical observations of the sulci or gyri (Rademacher, Galaburda, Kennedy, Filipek, & Caviness Jr., 1992), topographic landmark (Kim et al., 2000), and anatomical connectivity patterns (Xu et al., 2015). However, these studies based on different information identified different parcellation schemes for MTG, making functional organization of this area controversial. Moreover, the associations between these subregions of MTG and particular functions remain an open problem.

Connectivity-based parcellation (CBP) using resting-state functional magnetic resonance imaging (rs-fMRI) is a direct approach to identify the intrinsic functional organization of the brain (Fan et al., 2015; Kim et al., 2010). By using machine learning-related clustering approach, the voxels showing similar connectivity patterns were grouped into one cluster as a subregion of a specific brain area (Eickhoff, Yeo, & Genon, 2018; Wang, Fan, et al., 2015; Wang et al., 2018). With this approach, many brain areas including insula and inferior parietal lobule were parcellated into subregions (Cohen et al., 2008; Nelson, Cohen, et al., 2010; Nelson, Dosenbach, et al., 2010; Wang et al., 2012; Wang et al., 2017). Moreover, there was a good correspondence between the functional and anatomical connectivity patterns-based parcellation results (Kim et al., 2010; Wang et al., 2016, 2019). In spite of the similarity between the connectivity patterns defined using rs-fcMRI and diffusion MRI, structural and functional divergence has also been documented (Nebel et al., 2014; Vincent et al., 2007). Therefore, based on different resting-state functional connectivity (RSFC) patterns to define functional subregions of

MTG may provide additional information to better delineate the functional organization of this area.

In this study, we adopted the RSFC-based parcellation approach to define the intrinsic functional topography of the MTG and to determine whether functional organization was similar with structural delineation of this area. We further mapped the specific RSFC and coactivation patterns and characterized the detailed functions of each subregion. First, the bilateral MTGs were parcellated into component subregions using intrinsic RSFC patterns in two independent datasets. Next, whole brain RSFC and coactivation patterns, specific RSFC and coactivation patterns, and fingerprints with predefined 10 resting-state networks for each subregion were mapped. Finally, functional characterizations of each subregion using meta-analysis were performed to explore their detailed functions and behavioral profiles.

2 | MATERIALS AND METHODS

2.1 | Participants

Twenty-four healthy, right-handed subjects (12 males and 12 females, age range: 21–25 years) were recruited at Shenzhen Institutes of Advanced Technology, Chinese Academy of Sciences (Dataset 1). They are all Han-Chinese and not multilingual. No participants had a history of neurological and psychiatric disorders, and none had any contraindications for MRI scanning. This study was approved by the ethics committee of Institutional Review Board of Shenzhen Institutes of Advanced Technology, Chinese Academy of Sciences. Written informed consent was obtained from each participant. All methods were carried out in accordance with approved guidelines and regulations.

For validation, resting-state fMRI data of 10 healthy adults (age 22–25, 5 males) were downloaded from Q3 data release from the Human Connectome Project (HCP, <https://www.humanconnectome.org/>) database (Dataset 2).

2.2 | MRI data acquisition

The resting-state fMRI data for Dataset 1 were acquired using a Siemens 3 T MAGNETOM Trio scanner using an echo-planar imaging (EPI). The sequence parameters were as follows: 32 axial slices, acquisition matrix = 64×64 , repetition time (TR) = 2,000 ms, echo time (TE) = 30 ms, flip angle (FA) = 90° , size of voxel = $3.44 \times 3.44 \times 4.4$ mm, and slice thickness = 4 mm. Each condition consists of 240 functional volumes. During scanning, subjects were instructed to close their eyes, to relax, to think nothing, and to lie still.

The Dataset 2 were collected on a 3 T Skyra scanner (Siemens, Erlangen, Germany) using a 32-channel head coil. In this study, we chose the data from Session 1 with the left to right phase encoding. Parameters for these rs-fMRI data were: TR = 720 ms, TE = 33.1, FA = 52° , size of voxel = $2 \times 2 \times 2$ mm voxels, and 72 oblique axial slices. This functional run lasted 14.55 min (1,200 time points).

2.3 | Resting-state fMRI data preprocessing

Preprocessing of the Dataset 1 was performed using the Data Processing Assistant for Resting-State fMRI (DPARSF, <http://rfmri.org/DPARSF>). For each participant, the preprocessing steps include: (a) the first 10 volumes of each functional time-series were discarded to allow for magnetization equilibrium; (b) the slice times for the remaining 230 images were corrected and realigned to the first volume to account for head motion; (c) all data were spatially normalized to the Montreal Neurological Institute (MNI) template and resampled to $3 \times 3 \times 3 \text{ mm}^3$; (d) spatial smoothing was performed using a Gaussian kernel of 6 mm full-width at half maximum (FWHM); (e) temporal band-pass filtering (0.01–0.1 Hz) was performed; (f) white matter and cerebrospinal fluid signals, global mean signals, and six motion parameters were regressed out; and (g) the time course for each run was “scrubbed” by eliminating the bad images, captured before two time points and after one time points, which exceeded the preset criteria (frame displacement: FD, $FD < 0.5$) for excessive motion.

The fMRI data of Dataset 2 were downloaded in a preprocessed form after the minimal preprocessing pipeline (v. 3.2) (Glasser, et al., 2013). The main preprocessing steps were: First, these data were preprocessed using tools from FSL (<https://fsl.fmrib.ox.ac.uk/fsl/fslwiki/>) and FreeSurfer (<http://surfer.nmr.mgh.harvard.edu>) to implement gradient unwarping, motion correction, fiedmap-based EPI distortion correction, brain-boundary-based registration of EPI to a structural T1-weighted scan, nonlinear registration into MNI space, and grand-mean intensity normalization. Then, these data were further processed using FSL and the Analysis of Functional and NeuroImages (AFNI). The main steps were: (a) band-pass filtering of the time-series (0.01–0.1 Hz); (b) regressing the nuisance signals including the six rigid motion parameters, white matter mean signal, cerebrospinal fluid mean signal, and global mean signal; (c) spatial smoothing the residuals using a 4 mm FWHM Gaussian kernel; and (d) resample these images to $3 \times 3 \times 3 \text{ mm}^3$.

2.4 | Definition of the bilateral MTG seed masks

The bilateral MTG masks were defined using Harvard-Oxford cortical structural atlases in FSL software (<http://fsl.fmrib.ox.ac.uk/fsl/fslwiki/Atlases>). The definition of the bilateral MTG was the same with our previous study (Xu et al., 2015). Then, the bilateral MTG masks were resampled into $3 \times 3 \times 3 \text{ mm}^3$ in MNI space for the RSFC mapping, resulting 860 voxels for left MTG and 941 voxels for right MTG.

2.5 | RSFC-based parcellation

We used different RSFC patterns to identify the functional organization of bilateral MTGs. First, we calculated the functional connectivity between each voxel of the bilateral MTG and any other voxels of the rest of the brain for each subject and converted to z-score using a Fisher's z transformation. Then, we computed the similarity of functional connectivity maps for every pair of voxels within the MTG using

η^2 measurement (Cohen et al., 2008; Kelly et al., 2012; Wang, Yang, et al., 2015; Wang et al., 2016, 2017).

$$\eta^2 = 1 - \frac{SS_{\text{within}}}{SS_{\text{combined}}} = 1 - \frac{\sum_{i=1}^n (a_i - m_i)^2 + (b_i - m_i)^2}{\sum_{i=1}^n (a_i - \bar{M})^2 + (b_i - \bar{M})^2}$$

Where a_i and b_i are the values at position i in the functional connectivity maps a and b , respectively. The m_i is the mean value of the two functional connectivity maps at position i , and \bar{M} is the grand-mean across all locations in both correlation maps. The values of the correlation matrix are the fraction of the variance in one functional connectivity map accounted for by the variance in a second functional connectivity map. Next, the similarity matrix was segmented into different numbers of clusters (range from 2 to 6) using spectral clustering algorithm to define the subregions of the bilateral MTGs, which is the same with our previous studies (Xu et al., 2015).

2.6 | Maximum probability map

Given inter-individual differences in the MTG parcellation, we calculated the maximum probability map (MPM) to show the final results ($N = 2, 3, \dots, 6$) for the two datasets, separately. The MPM was calculated in the MNI space by assigning each voxel to the subregion to which it was most likely to belong (Wang et al., 2012).

2.7 | Determining the number of clusters

How to determine the optimal parcellation solutions for brain areas is very hard. In this study, we used hierarchy index (HI) which reflects the hierarchical structure of the different solutions by the average probability that a given cluster in k solution has only one “parent-cluster” in $k - 1$ solution (Kahnt, Chang, Park, Heinzle, & Haynes, 2012; Li et al., 2017) to select the final parcellation results. Specifically, HI is defined

as $HI_k = \frac{1}{k} \sum_{i=1}^k \frac{\max(x_{ij})}{x_i}$, where $\bar{x}_i = \sum_{j=1}^{k-1} x_{ij}$, here x is a matrix whose elements

x_{ij} reflects the number of voxels in cluster $j_{i=1..k}$ stemming from cluster $j_{i=1..k-1}$ in $k-1$ solution ($K > 2$). HI values of 1 means a perfect hierarchical structure of a brain region. Thus, the maximum HI values were used for choosing optimal parcellation results for bilateral MTG.

To validate our results, we also used the Dice coefficient to calculate the similarity between parcellation results yielded by the two independent datasets (Dataset 1 and Dataset 2) with number of clusters ranging from 2 to 6. Dice Coefficient was defined by $2 * (|A \cap B|) / (|A| + |B|)$, where A and B are the total voxels for a specific subregion in the two datasets. The mean overlap degree for left and right MTG was calculated to show the parcellation similarity.

2.8 | Overlapping with DTI-based parcellation results

We compared our parcellation results using resting-state fMRI with the parcellation results of MTG obtained by DTI-based parcellation in

our previous work (Xu et al., 2015). An overlapped map was obtained between RSFC-based and DTI-based parcellation results of the MTG, and the overlap degree was calculated for each subregion using the Dice coefficient to quantitatively measure the similarity.

2.9 | The whole brain RSFC patterns

The RSFC was defined as the Pearson correlation coefficients between the mean time-series of each seed region (thresholded at 50% probability) and that of each voxel in the rest brain. Correlation coefficients were converted to z values using Fisher's z transformation to improve normality. Next, one-sample t -tests were performed to identify voxels which showed significant correlations with the seed region in these normalized correlation maps. For all the above voxel-wise comparisons, a significance threshold was set at a cluster-level of $p < .05$, family wise error (FWE)-corrected, cluster-forming threshold at voxel-level $p < .001$.

2.10 | The whole brain coactivation patterns

To obtain the task-dependent coactivation patterns of each subregion (thresholded at 50% probability), we used structure-based meta-analysis and meta-analytic connectivity modeling (MACM) approaches in the BrainMap database (<http://brainmap.org/>) by creating likelihood estimation (ALE) maps. The ALE scores were compared to a null-distribution reflecting a random spatial association between experiments with a fixed within-experiment distribution of foci (Tench, Tanasescu, Auer, Cottam, & Constantinescu, 2014), yielding a P -value based on the proportion of equal or higher random values (Eickhoff, Bzdok, Laird, Kurth, & Fox, 2012). These nonparametric P -values were converted to z -scores and corrected with a cluster-level FWE at the threshold of $p < .05$ (a voxel-level $p < .001$).

2.11 | Overlap analyses between RSFC and coactivation patterns

In order to identify the common network shared by the whole brain RSFC patterns and coactivation patterns of each subregion, we initially computed and thresholded whole brain RSFC and task-related coactivation networks for each MTG subregion, as described above. Finally, a conjunction analysis (i.e., the intersection connectivity analysis) was performed to calculate the overlap between the two thresholded networks (task-related coactivation network and resting-state network) for each subregion.

2.12 | Special RSFC and coactivation pattern for each subregion

We also mapped the specific network for each subregion to reveal the unique RSFC and coactivation patterns. The specific networks were the brain areas that were significantly more coupled and correlated with a given subregion than with any of the others.

2.13 | RSFC patterns with 10 predefined resting-state networks

To better understand the function of the MTG subregion, fingerprint analysis was also performed. First, we defined 10 resting-state brain networks based on a previous study which used independent component analysis (ICA) and identified 10 intrinsic networks of the human brain, including visual network (VN) 1, VN 2, VN 3, default mode network (DMN), cerebellum, sensorimotor network (SMN), auditory network (AN), executive control network (ECN), frontoparietal network (FPN), and cognition-language network (CLN). Then, the 10 brain networks were resampled to a voxel size resolution of 3 mm. Finally, the RSFCs between each MTG subregion (thresholded at 50% probability) and the 10 brain networks were calculated.

2.14 | Functional characterization using meta-analysis

To delineate the functions of each MTG subregion, we characterized the functional profiles as determined by forward and reverse inference in the BrainMap database with respect to the behavioral domain and paradigm class (Bzdok, Laird, Zilles, Fox, & Eickhoff, 2013; Clos, Amunts, Laird, Fox, & Eickhoff, 2013). In the forward inference approach, a subregion's functional profile was determined by identifying the taxonomic labels (domains or subdomains), for which the probability of finding activation in a specific subregion was significantly higher than the overall chance (across the entire database) of finding activation in that particular subregion. In the reverse inference approach, a subregion's functional profile was determined by identifying the most likely behavioral domains and paradigm classes given activation in a particular subregion using Bayies' rule. Significance of both methods was established using a binomial test ($p < .05$ corrected for multiple comparisons using the false discovery rate [FDR] method).

3 | RESULTS

3.1 | Parcellation of the MTG

The MTG was parcellated into 2 to 6 different clusters for the two datasets, separately. The MPM for each left and right MTG subregion at each solution was calculated and shown in Figure 1a for Dataset 1 and Figure S1a for Dataset 2.

The HI was used to choose the optimal number of clusters and the highest values were for $k = 4$ (Figure 1b). Thus, the four-way solutions were determined as the optimal number of subregions in bilateral MTG (Figure 1c) and used in the following analyses.

Moreover, we also used Dataset 2 to validate our results. The overlap degree between the two datasets further supported four-way parcellation as the optimal number of subregions in bilateral MTG (Figure S1b). The mean overlap maps of the four clusters between the two datasets were calculated (Figure S1c). The MTG subregions showed a comparable high level of consistency (overlap degree >0.5).

FIGURE 1 Middle temporal gyrus (MTG) parcellation results using resting-state functional connectivity (RSFC). (a) RSFC was used to parcellate the left MTG and right MTG into different numbers of clusters (2–6), respectively, in the Dataset 1. And the maximum probability map (MPM) for each MTG subregions at each solution was calculated. (b) Hierarchy index (HI) as a function of K , reflecting the hierarchical structure of the different solutions by the average probability that a given cluster in K has only one “parent-cluster” in $K - 1$ was calculated to choose the optimal parcellation results. The highest values were for $K = 4$. Thus, the four-way solutions were determined as the optimal number of subregions in bilateral MTG (c) and used in the following analyses [Color figure can be viewed at wileyonlinelibrary.com]

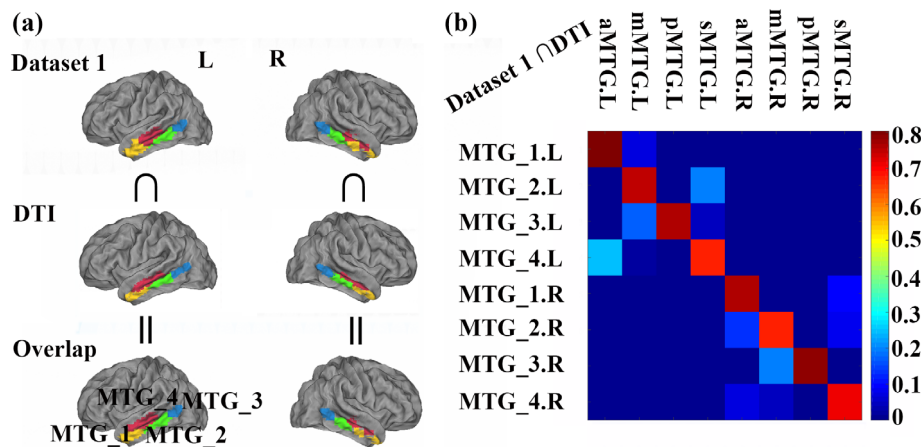
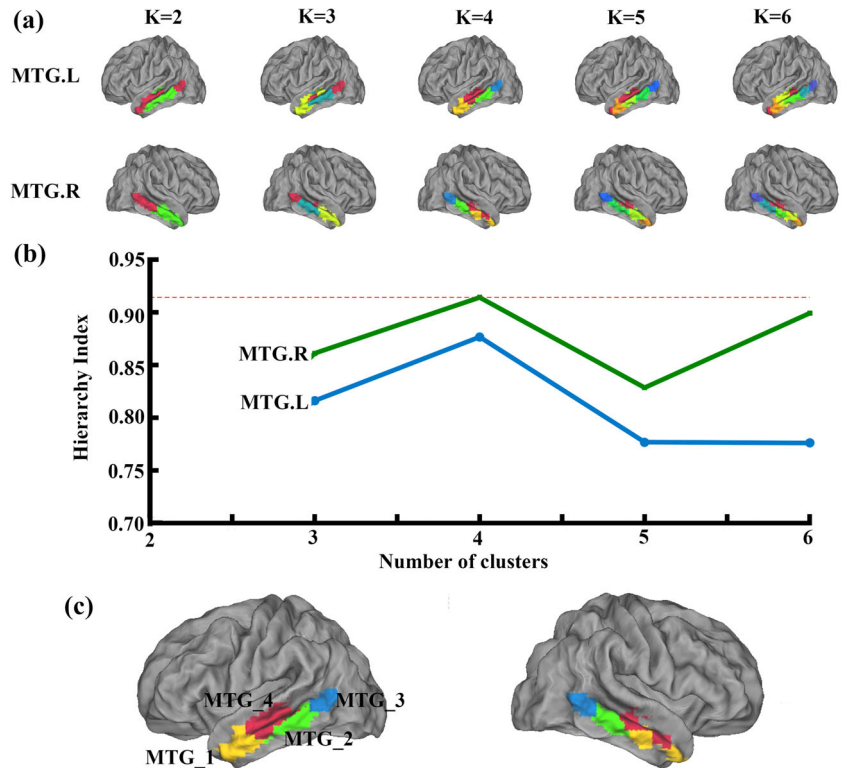


FIGURE 2 Overlap with the DTI-based parcellation results. (a) The overlap between the parcellation results obtained using the resting-state functional connectivity (RSFC) of the Dataset 1 and anatomical connectivity-based parcellation were calculated. The anatomical connectivity-based parcellation results of the bilateral middle temporal gyrus (MTG) were defined from our previous work (Xu et al., 2015). (b) The quantitative overlap analyses between RSFC-based parcellation of MTG results and that defined using anatomical connectivity-based parcellation were calculated. The overlap analyses identified a high overlap between the parcellation results using different modalities [Color figure can be viewed at wileyonlinelibrary.com]

3.2 | Overlapping with DTI-based parcellation

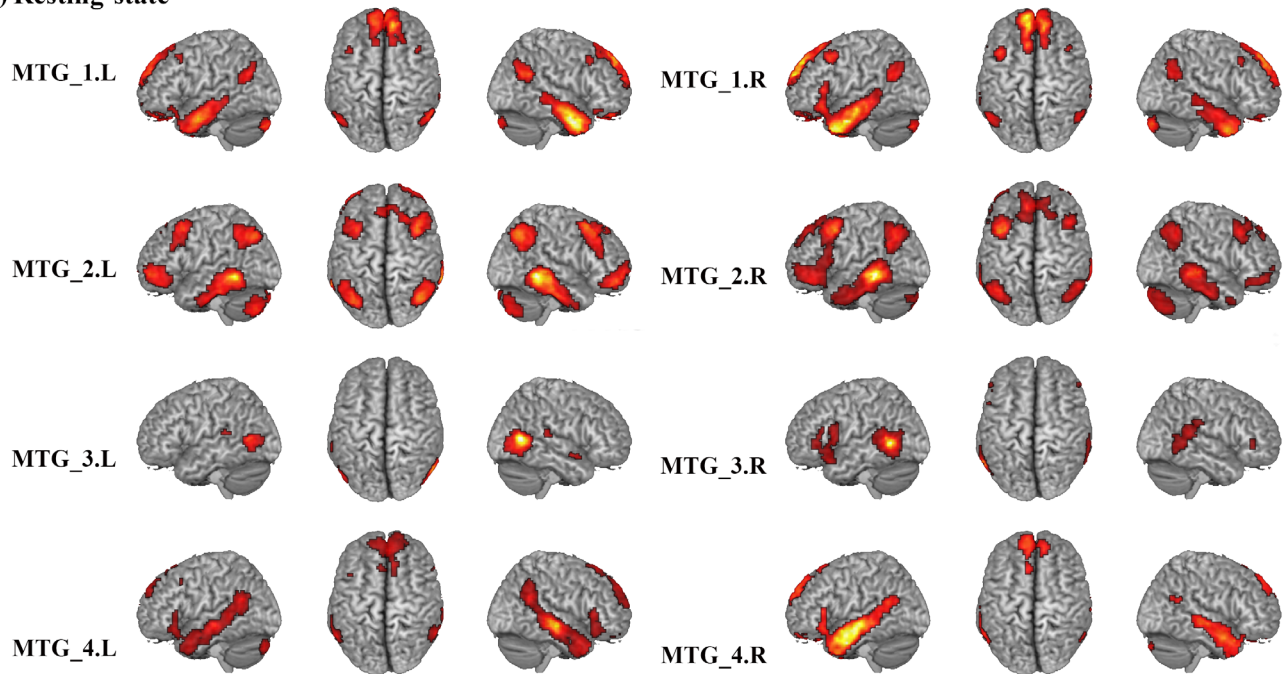
An overlap map was obtained between RSFC of Dataset 1 and DTI-based parcellation results of MTG (Figure 2a). The overlap degree between the parcellation results obtained using resting-state and DTI-based parcellation were also calculated and shown in Figure 2b. Although these two datasets were obtained from different sites, the quantitative analysis revealed a similar topographic pattern of MTG defined using different connectivity patterns. The parcellation of MTG identified three distinct clusters from anterior to posterior (MTG_1, MTG_2, and MTG_3) located in the gyrus, and one cluster

mainly located in the sulcus (MTG_4). In addition, all MTG subregions showed a comparable high level of consistency (overlap degree >0.67, the highest value was 0.8037).

3.3 | Whole brain RSFC patterns of the MTG subregions

Functional connectivity network for each MTG subregion was mapped and shown in Figure 3a and Table S1. From the RSFC pattern of each subregion, we found that the left MTG_1 was mostly

(a) Resting-state



(b) Coactivation

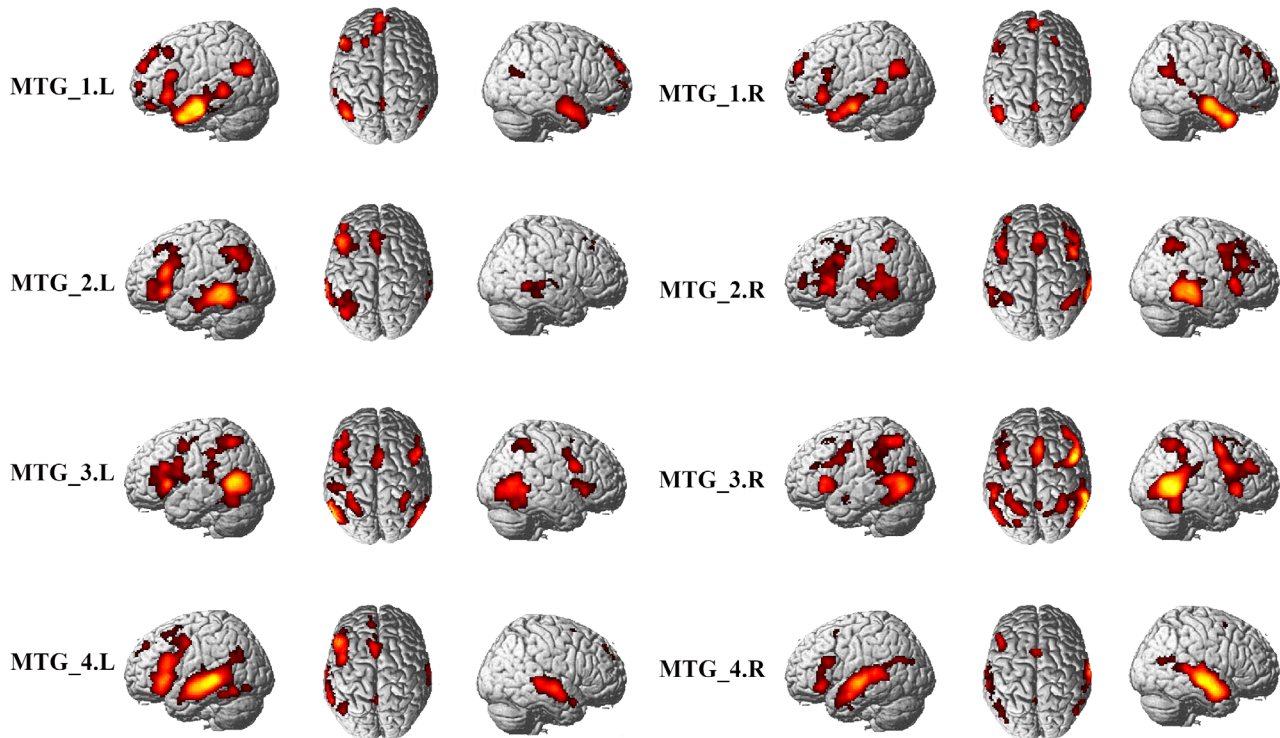


FIGURE 3 Whole brain resting-state functional connectivity (RSFC) and coactivation analysis for each middle temporal gyrus (MTG) subregion. (a). Whole brain RSFC patterns were obtained using one-sample *t*-tests. (b). The whole brain coactivation pattern for each MTG subregion was obtained using meta-analytical connectivity modeling (MACM) analyses. Both significance levels were set at $p < .05$, cluster-level FWE-corrected, cluster-forming threshold at voxel-level $p < .001$ [Color figure can be viewed at wileyonlinelibrary.com]

correlated with bilateral cerebellum, bilateral inferior temporal gyrus (ITG), right precuneus (PCun), right rectus, bilateral parahippocampal gyrus (ParaHIPP), bilateral angular gyrus (AG), and left middle frontal gyrus (MFG). The left MTG₂ was primarily correlated with the

bilateral cerebellum, bilateral MTG, bilateral orbital part of middle frontal gyrus (MFG_Orb), bilateral MFG, right middle cingulate cortex (MCC), left inferior parietal lobule (IPL), and bilateral AG. The left MTG₃ was correlated with bilateral MTG. The functional

connectivity pattern of the left MTG_4 was correlated with the left cerebellum, bilateral MTG, right triangle part of inferior frontal gyrus (IFG_Tri), right anterior cingulum cortex (ACC), and right PCun. The right MTG_1 was primarily correlated with the bilateral cerebellum, bilateral ITG, left SFG_Med, right ParaHIPP, left rectus, left post cingulate cortex (PCC), bilateral AG, and left MFG. The brain regions correlated with the right MTG_2 were found in the bilateral cerebellum, bilateral MTG, bilateral MFG, right MFG_Orb, left AG, right IPL, and right medial superior frontal gyrus (SFG_Med). The right MTG_3 correlated with the left MTG, left pole part of superior temporal gyrus (STG_Pole), and right STG. The functional connectivity pattern of the right MTG_4 was correlated with left ITG, right MTG, left SFG_Med, left rectus, and left PCun.

3.4 | Whole brain coactivation patterns of the MTG subregions

The whole brain coactivation patterns for the bilateral MTGs were mapped using MACM analysis and were displayed in Figure 3b and Table S2. The coactivation of the left MTG_1 was found in bilateral MTG, right hippocampus (HIPP), left orbital part of medial frontal gyrus (MedFG_Orb), left PCun, left MFG, left AG, left SFG_Med, and right middle occipital gyrus (MOG). For the left MTG_2, the coactivation was primarily observed in bilateral MTG, left HIPP, left IFG_Tri, left caudate, left SFG_Med. The left MTG_3 primarily coactivated with the bilateral MTG, bilateral insula, bilateral IFG_Oper, left supramarginal gyrus (SMG), bilateral IPL, and right supplementary motor area (SMA). The coactivated brain regions with the left MTG_4 was found in the left MTG, right STG, left IFG_Tri, left ANG, left SFG_Med, and left SMA. The coactivation pattern for the right MTG_1 was predominately identified in bilateral MTG, left HIPP, bilateral IFG_Orb, left PCC, left SFG_Med, left ANG, and right SFG. The coactivation of the right MTG_2 was mainly found in bilateral MTG, bilateral insula, left SFG_Med, right AG, and left IPL. The coactivation pattern of the right MTG_3 was mainly observed in the right MTG, left amygdala, left insula, bilateral thalamus, the right IFG_Oper, right MOG, left precentral gyrus (PreCG), left SMA, left SPL, and left PCun. The coactivated brain regions for the right MTG_4 was found in the right MTG, left STG, bilateral HIPP, right IFG_Orb, left PCun, and left SMA.

3.5 | Intersection of the RSFC and coactivation patterns

In order to explore the correspondent connectivity profiles of each MTG subregion at rest and under task, we calculated the intersection map of the thresholded whole brain RSFC and coactivation patterns (Figure 4 and Table S3). The conjunction of the left MTG_1 was found in bilateral ITG, bilateral ParaHIPP, right rectus, left IFG_Orb, right PCun, left AG, right STG, and left SFG. For the left MTG_2, the shared RSFC and coactivation was primarily observed in bilateral MTG, left IFG_Orb, left MFG, left AG, and left SFG_Med. The overlap between rest and task of the left MTG_3 was only found in

bilateral MTG. For the left MTG_4, the overlap between rest and task was found in bilateral MTG, left IFG_Orb, left ANG, right PCun, and left SFG_Med. The conjunct connectivity of the right MTG_1 was found in bilateral MTG, bilateral ITG, bilateral ParaHIPP, left rectus, left IFG_Orb, left SFG_Med, bilateral AG, and left PCC. For the right MTG_2, the conjunction was observed in bilateral MTG, left IFG_Orb, left orbital part of middle frontal gyrus (MFG_Orb), bilateral MFG, left SMA, and left IPL. The overlap between rest and task of the right MTG_3 was found in left MTG, right STG, left IFG_Oper, and left IFG_Orb. For the right MTG_4, the overlap was found in bilateral MTG, left ParaHIPP, left IFG_Tri, bilateral STG, and left PCun.

3.6 | Specific connectivity of each MTG subregion

We mapped the overlap between the specific whole brain RSFC and coactivation connectivity to identify the specific network that each MTG subregion participated in (Figure 5 and Table S4). The specific connectivity of the left MTG_1 was found in right MTG, bilateral ParaHIPP, left ITG, bilateral MTG_Pole, right rectus, left SFG_Med, right PCun, left ANG, and left SFG. For the left MTG_2, the specific connectivity was primarily observed in bilateral MTG, left IFG_Orb, left SFG_Med, IPL, and left MFG. The specific connectivity for the left MTG_3 was found in the bilateral MTG. The left MTG_4 specifically connected with left STG_Pole, left MTG, and bilateral STG. The specific functional connectivity for the right MTG_1 was predominately observed in bilateral ITG, bilateral ParaHIPP, right SFG_Med, right PCC, left MTG, and right AG. For the right MTG_2, the specific connectivity was primarily observed in bilateral MTG, left MFG_Orb, left IFG_Tri, left PreCG, right MFG, and bilateral IPL. The specific connectivity for right MTG_3 was mainly found in left MTG and right STG. The specific connectivity for the right MTG_4 was mainly observed in left MTG and right STG.

3.7 | RSFC with 10 predefined brain networks

The fingerprint of each MTG subregion was mapped by calculating the RSFC of each MTG subregion with 10 predefined brain networks (Figure 6). In summary, the MTG_1 was mainly correlated with DMN and FPN. The MTG_2 was mainly correlated with SMN, ECN, and CLN. The left MTG_3 was mainly correlated with VN 3 and ECN, whereas the right MTG_3 was mainly correlated with VN 3, AN, and CLN. The MTG_4 was mainly correlated with FPN and AN.

3.8 | Functional characterization

The quantitative forward and reverse inferences on the behavioral domains and paradigm classes were applied and revealed that different subregions participated in different cognitive functions (Figure 7).

In summary, the functions that were significantly associated with the left MTG_1 were memory (memory explicit), language, and social cognition. The left MTG_2 was significantly associated with social cognition and language semantics. For the left MTG_3, the significantly associated functions were language semantics and action

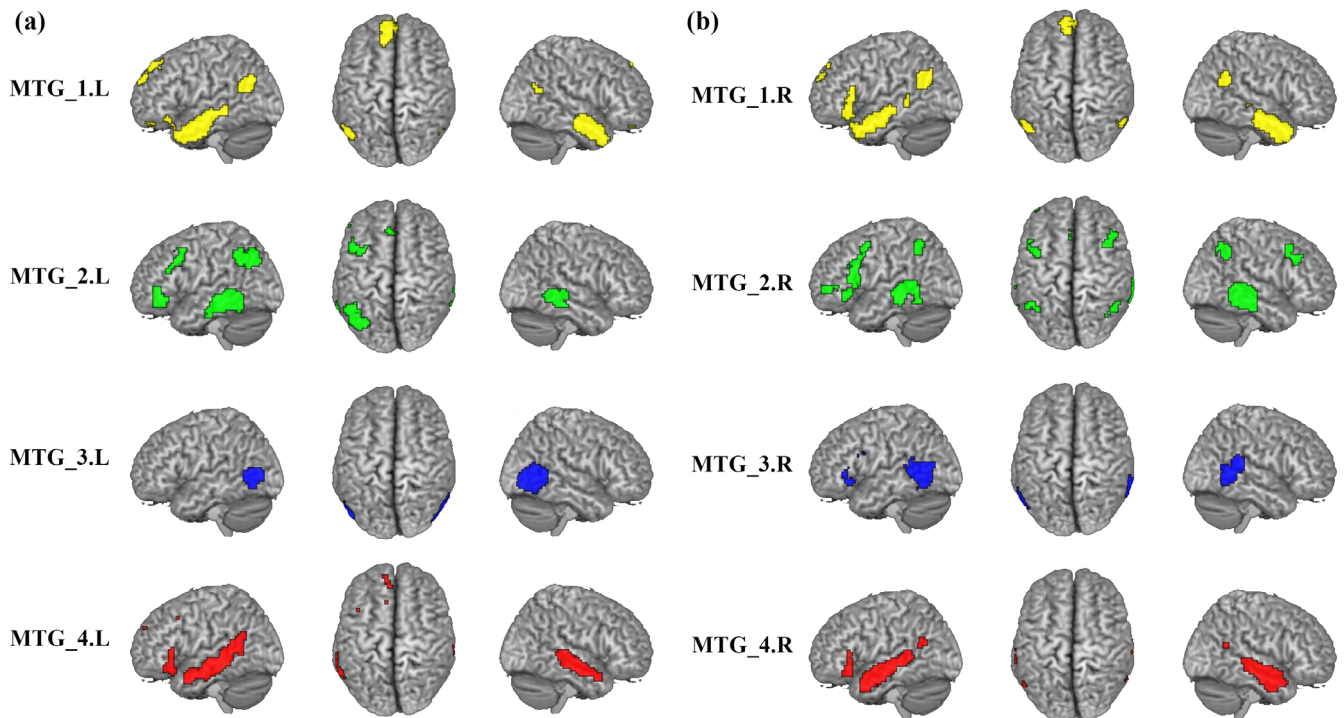


FIGURE 4 Overlapped connectivity between resting-state functional connectivity (RSFC) and coactivation patterns. The intersection connectivity between thresholded whole brain RSFC and coactivation for each middle temporal gyrus (MTG) subregion was computed [Color figure can be viewed at wileyonlinelibrary.com]

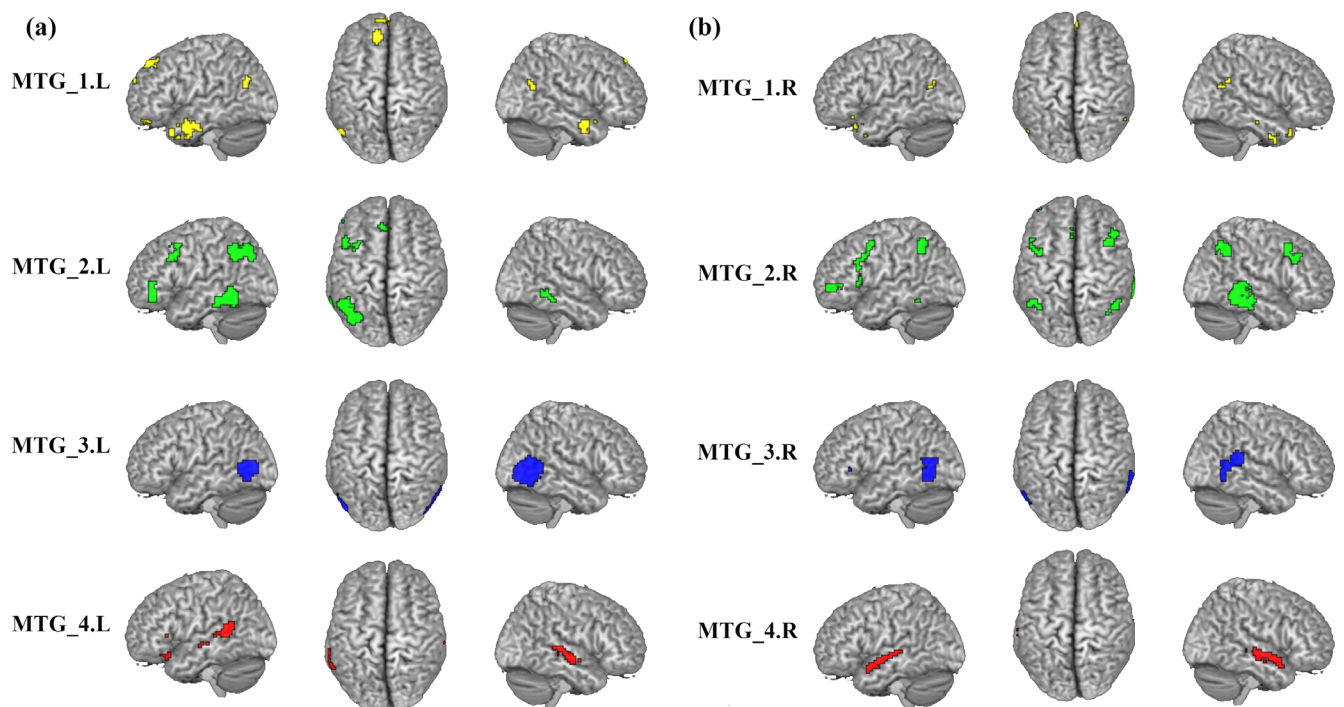


FIGURE 5 The specific functional patterns for the middle temporal gyrus (MTG) subregion. The brain areas show significantly more correlated and coupled with a given subregion than with any of the other MTG subregions [Color figure can be viewed at wileyonlinelibrary.com]

observation. The left MTG_4 was only significantly associated with various language processing, audition, and social cognition. The right MTG_1 was significantly associated with emotion (Emotion

happiness), social cognition, memory explicit, and language. The main function of the right MTG_2 was audition. For the right MTG_3, the significantly associated function was action observation. The right

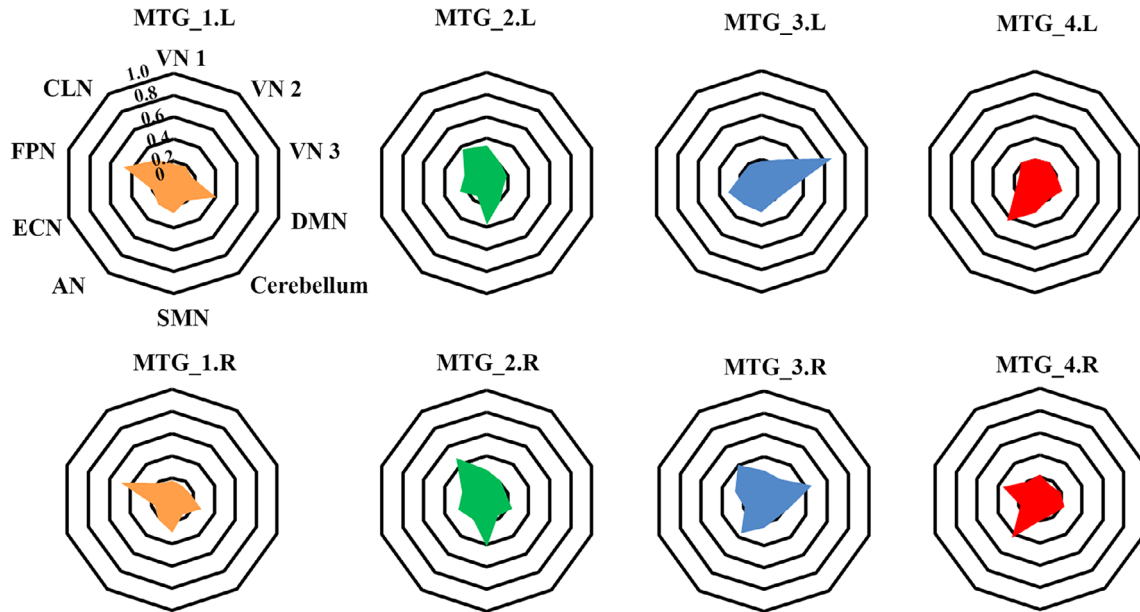


FIGURE 6 Fingerprints of the middle temporal gyrus (MTG) subregions with ten predefined brain networks. We first defined ten brain networks according to a previous study (Smith et al., 2009). Then, the resting-state functional connectivities (RSFCs) between each MTG subregion and the 10 brain networks were calculated and averaged across all the subjects [Color figure can be viewed at wileyonlinelibrary.com]

MTG_4 was significantly associated with language, audition, and social cognition. The reverse inference showed similar patterns.

4 | DISCUSSION

In this study, we parcellated the bilateral MTG into four distinct subregions based on their distinct functional connectivity profiles using two independent datasets. Our results yield a similar topographic pattern defined by anatomical CBP. We also found that each MTG subregion had its specific connectivity patterns, and was involved in different task-related behaviors.

Different neuroimaging modalities and techniques have been used to parcellate the bilateral MTG. However, most previous parcellation of MTG was either based on myelo- or cyto-architectonic information or anatomical information (Kim et al., 2000; Rademacher et al., 1992; Searwards, 2011; Yates et al., 2006), which mainly focused on internal microstructure of the brain while lacking of connectivity information. Based on different anatomical connectivity patterns, the MTG was subdivided into 4 distinct subregions (aMTG, mMTG, pMTG, and sMTG) in our previous work (Xu et al., 2015). In the current study, we used RSFC to explore the functional segregations of the MTG and identified a similar pattern with four distinct clusters (MTG_1, MTG_2, MTG_3, and MTG_4). Compared with anatomical CBP of the MTG, MTG_1, MTG_2, MTG_3, MTG_4 in our study was mainly corresponding to the aMTG, mMTG, pMTG, and sMTG, respectively. Moreover, all MTG subregions showed a comparable high level of consistency (overlap degree >0.67). These similarities supported the view that the functional connectivity is likely mediated by anatomical connectivity (Deco, Jirsa, & McIntosh, 2011; Wig, Schlaggar, & Petersen, 2011), and that structure and function are closely related in

brain architecture. However, difference between the parcellation results obtained with RSFC and anatomical connectivity was also existed. The difference may result from different datasets, different methodologies and their inherent limitations. In fact, the anatomical connectivity primarily reflects direct axonal connections, while the functional connectivity enables not only identification of direct axonal connections but also characterization of the indirect axonal connections between brain areas (Barttfeld et al., 2015). Therefore, it is possible for differential functional zones to exist even within an area that shares gross similarities in anatomy.

Connectivity and coactivation mapping with functional characterization revealed different MTG subregions involving in different functions in this study. The left MTG subregions were mainly participated in various languages processing, including phonological discrimination, semantic monitor, reading, and word generation, but in the right hemisphere, only the right MTG_4 was involved in phonological discrimination. These results not only supported previous finding that the left MTG plays a critical role in almost all domains of language processing (Floel et al., 2001; Gutierrez-Sigut, Payne, & MacSweeney, 2015; Knecht et al., 2000), but also strongly confirmed the left lateralized aspect of the language processing (BullaHellwig, Vollmer, Gotzen, Skreczek, & Hartje, 1996; Vingerhoets & Stroobant, 1999).

Specially, the bilateral MTG_1 mainly connected with left PCun and SFG_Med, two key nodes of the DMN (Gusnard, Akbudak, Shulman, & Raichle, 2001a; Gusnard, Akbudak, Shulman, & Raichle, 2001b; Raichle et al., 2001). This was further confirmed by fingerprints analysis which showed high functional connectivity between MTG_1 and DMN. These results further supported the finding that the MTG_1 was a critical part of DMN, which was similar with the aMTG defined using anatomical CBP in our previous study. In

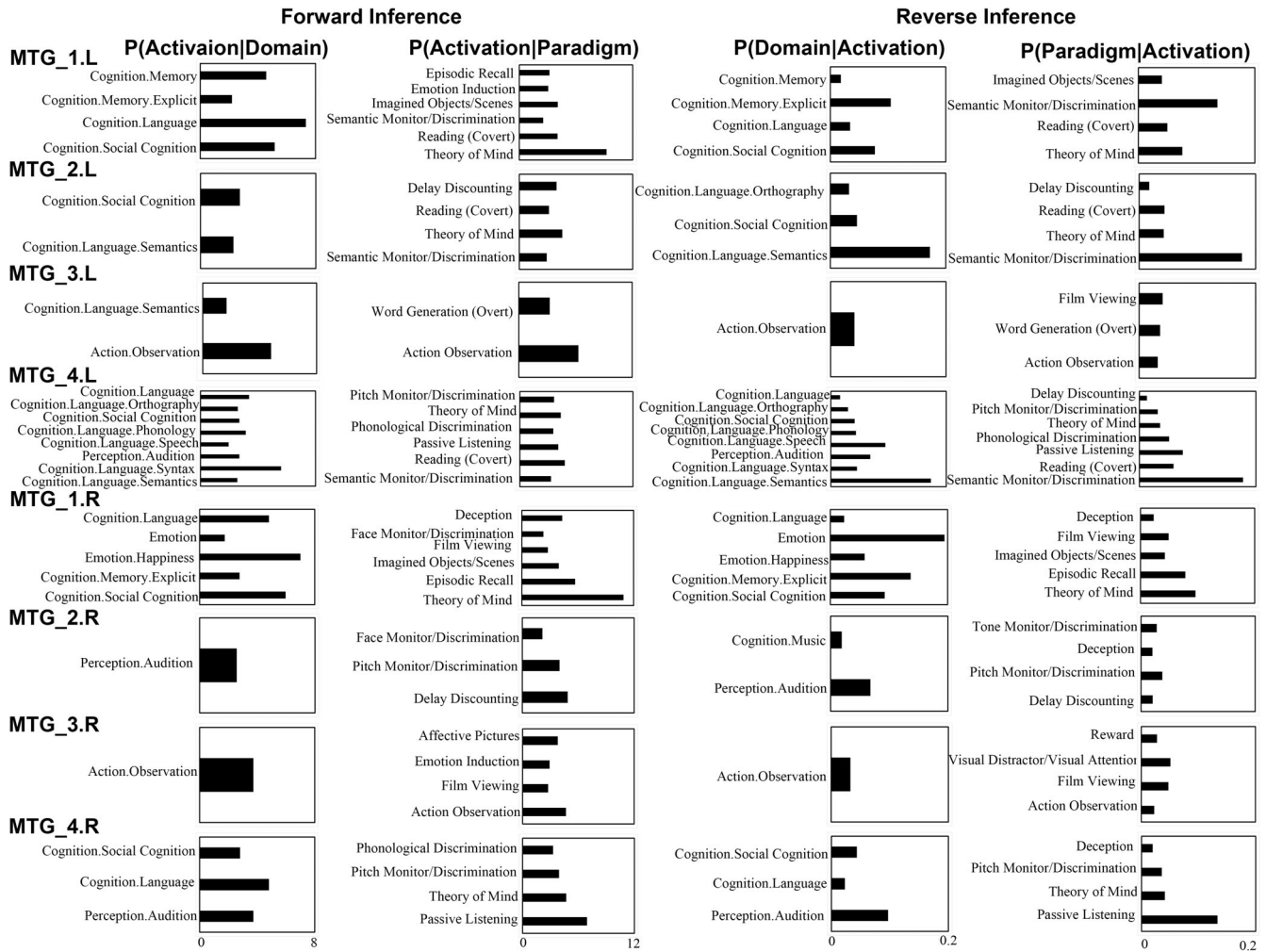


FIGURE 7 Functional characterizations of the middle temporal gyrus (MTG) subregions. Forward and reverse inferences were used to determine the functions of each subregion. The significant activation probabilities for each subregion with respect to a given domain or paradigm and the significant probability of a domain's or paradigm's occurrence given activation in a specific subregion are depicted, separately

addition, the functional characterization showed that the left MTG_1 were also involved in semantic processing and explicit memory. Given the explicit memory includes episodic memory and semantic memory, thus, left MTG_1 might be also associated with semantic memory. Our findings, together with previous studies (Binder, Desai, Graves, & Conant, 2009; Wirth et al., 2011), suggested that the SM and DMN were spatially overlapped in the left MTG_1.

In addition, bilateral anterior MTG subregions (MTG_1.L, MTG_2.L, MTG_4.L, MTG_1.R, and MTG_4.R) were also involved in the social cognition, that is, theory of mind (ToM). The ToM is a function that can infer the others' behaviors and mental states (Koster-Hale & Saxe, 2013; Molenberghs, Trautwein, Bockler, Singer, & Kanske, 2016; Schurz, Radua, Aichhorn, Richlan, & Perner, 2014). Typically, ToM network mainly includes the bilateral temporo-parietal junction, medial prefrontal cortex, and PCun. But, increasing studies reported that the MTG is also a key component of the ToM network. For example, a study on social animations compared to false belief showed the strongest activation in the MTG (Schurz, Tholen, Perner, Mars, & Sallet, 2017). Schurz et al. (2014) found significant activation during the

tasks of social animations and mind in the eyes in the MTG. Our current results suggested that the anterior MTG might be involved in the ToM network.

The functional decoding for bilateral MTG_3 found that both areas participated in action observation. Many studies demonstrated that the posterior MTG was involved in perception (Beauchamp & Martin, 2007; Iacoboni et al., 2005), observing objects (Valyear & Culham, 2010), physical constraints (i.e., a barrier determining the height of the arm trajectory for reaching an object; Jastorff, Clavagnier, Gergely, & Orban, 2011), and providing information related to the observed object and associated actions (Kilner, 2011). Moreover, it has been reported that the left posterior MTG showed increased activity as the number of possible implied actions related to the observed object augments (Schubotz, Wurm, Wittmann, & von Cramon, 2014). Recently, posterior MTG was also identified to be involved in coding objects' appropriate grasp ability (Amoruso, Finisguerra, & Urgesi, 2018). All the evidence suggested that the posterior MTG might play a critical part in integrating the motoric details of the action with stored semantic knowledge about the objects. Therefore, the previously identified MTG in the

action observation might be confined to MTG_3. This conclusion was also supported by the connectivity patterns of this area which coactivated with the left PreCG/the left SMA, and had higher RSFC with AN.

There are also limitations in our current study. First, we used a 6 mm FWHM smoothing in the fMRI data processing of the Dataset 1 to improve the signal-to-noise ratio, which is the same with previous studies (Kelly et al., 2012; Mishra, Rogers, Chen, & Gore, 2014). However, the fMRI data of the Dataset 2 were smoothed by 4 mm FWHM and then resampled to $3 \times 3 \times 3$ mm since the original resolution was $2 \times 2 \times 2$ mm. Thus, we cannot exclude the potential effects of the different smoothing kernels on the results. Finally, our parcellation results were based on RSFC, a new parcellation technique is needed to verify our results, such as dynamic functional connectivity-based on resting-state fMRI (Ji et al., 2016), which might be helpful to further uncover the functional segregations of the MTG at a different level.

5 | CONCLUSION

In conclusion, we demonstrated a similar pattern of MTG defined using RSFC-based parcellation with that yielded by anatomical CBP. Parcellation of the bilateral MTGs identified four subregions with three clusters from anterior to posterior located in the gyrus, and one cluster mainly located in the sulcus. The resulting subregions feature distinct RSFC and coactivation connectivity patterns, different fingerprints and functional involvement. Our findings provide more detailed information about the functional organization of the MTG and may facilitate future clinical and cognitive research on this area.

ACKNOWLEDGMENTS

This work was supported by the Natural Science Foundation of Guangdong Province (No. 2017A030313744), the Science and technology innovation program of Shenzhen (No. JCYJ20160531184531506), National Natural Science Foundation of China (61671440, U1713215, 61701078), Shenzhen Key Basic Research Grant (JCYJ20160331191401141, and KQJSCX20170731162830878).

CONFLICT OF INTERESTS

The authors declare that they have no conflict of interest.

DATA AVAILABILITY STATEMENT

The Dataset 1 are in house dataset and are available from the corresponding author upon reasonable request. The Dataset 2 is openly available in HCP (<https://www.humanconnectome.org/>).

ORCID

Jinping Xu  <https://orcid.org/0000-0001-9175-2598>

Jiaojian Wang  <https://orcid.org/0000-0002-0421-5709>

REFERENCES

- Amoruso, L., Finisguerra, A., & Urgesi, C. (2018). Contextualizing action observation in the predictive brain: Causal contributions of prefrontal and middle temporal areas. *NeuroImage*, *177*, 68–78.
- Assaf, M., Hyatt, C. J., Wong, C. G., Johnson, M. R., Schultz, R. T., Hendler, T., & Pearlson, G. D. (2013). Mentalizing and motivation neural function during social interactions in autism spectrum disorders. *NeuroImage: Clinical*, *3*, 321–331.
- Barttfeld, P., Uhrig, L., Sitt, J. D., Sigman, M., Jarraya, B., & Dehaene, S. (2015). Signature of consciousness in the dynamics of resting-state brain activity. *Proceedings of the National Academy of Sciences of the United States of America*, *112*, 887–892.
- Beauchamp, M. S., & Martin, A. (2007). Grounding object concepts in perception and action: Evidence from fMRI studies of tools. *Cortex*, *43*, 461–468.
- Binder, J. R., Desai, R. H., Graves, W. W., & Conant, L. L. (2009). Where is the semantic system? A critical review and meta-analysis of 120 functional neuroimaging studies. *Cerebral Cortex*, *19*, 2767–2796.
- Bozkurt, B., Centeno, R. D., Chaddad-Neto, F., da Costa, M. D. S., Goiri, M. A. A., Karadag, A., ... Grande, A. (2016). Transcortical selective amygdalohippocampectomy technique through the middle temporal gyrus revisited: An anatomical study laboratory investigation. *Journal of Clinical Neuroscience*, *34*, 237–245.
- Bujarski, K. A., Hirashima, F., Roberts, D. W., Jobst, B. C., Gilbert, K. L., Roth, R. M., ... Thadani, V. M. (2013). Long-term seizure, cognitive, and psychiatric outcome following trans-middle temporal gyrus amygdalohippocampectomy and standard temporal lobectomy. *Journal of Neurosurgery*, *119*, 16–23.
- BullaHellwig, M., Vollmer, J., Gotzen, A., Skreczek, W., & Hartje, W. (1996). Hemispheric asymmetry of arterial blood flow velocity changes during verbal and visuospatial tasks. *Neuropsychologia*, *34*, 987–991.
- Bzdok, D., Laird, A. R., Zilles, K., Fox, P. T., & Eickhoff, S. B. (2013). An investigation of the structural, connective, and functional subspecialization in the human amygdala. *Human Brain Mapping*, *34*, 3247–3266.
- Cheng, C., Dong, D., Jiang, Y., Ming, Q., Zhong, X., Sun, X., ... Yao, S. (2019). State-related alterations of spontaneous neural activity in current and remitted depression revealed by resting-state fMRI. *Frontiers in Psychology*, *10*, 245.
- Clos, M., Amunts, K., Laird, A. R., Fox, P. T., & Eickhoff, S. B. (2013). Tackling the multifunctional nature of Broca's region meta-analytically: Coactivation-based parcellation of area 44. *NeuroImage*, *83*, 174–188.
- Cohen, A. L., Fair, D. A., Dosenbach, N. U. F., Miezin, F. M., Dierker, D., Van Essen, D. C., ... Petersen, S. E. (2008). Defining functional areas in individual human brains using resting functional connectivity MRI. *NeuroImage*, *41*, 45–57.
- Deco, G., Jirsa, V. K., & McIntosh, A. R. (2011). Emerging concepts for the dynamical organization of resting-state activity in the brain. *Nature Reviews Neuroscience*, *12*, 43–56.
- Eickhoff, S. B., Bzdok, D., Laird, A. R., Kurth, F., & Fox, P. T. (2012). Activation likelihood estimation meta-analysis revisited. *NeuroImage*, *59*, 2349–2361.
- Eickhoff, S. B., Yeo, B. T. T., & Genon, S. (2018). Imaging-based parcellations of the human brain. *Nature Reviews Neuroscience*, *19*, 672–686.
- Fan, J. E., Zhong, M. T., Gan, J., Liu, W. T., Niu, C. Y., Liao, H. Y., ... Zhu, X. Z. (2017). Spontaneous neural activity in the right superior temporal gyrus and left middle temporal gyrus is associated with insight level in obsessive-compulsive disorder. *Journal of Affective Disorders*, *207*, 203–211.
- Fan, Y., Nickerson, L. D., Li, H., Ma, Y., Lyu, B., Miao, X., ... Gao, J. H. (2015). Functional connectivity-based Parcellation of the thalamus: An unsupervised clustering method and its validity investigation. *Brain Connectivity*, *5*, 620–630.

- Floel, A., Knecht, S., Lohmann, H., Sommer, J., Drager, B., Buyx, A., ... Henningsen, H. (2001). Reproducibility of functional transcranial Doppler sonography in determining lateralization of visuospatial attention. *NeuroImage*, *13*, S314–S314.
- Friedman, L., Kenny, J. T., Wise, A. L., Wu, D., Stuve, T. A., Miller, D. A., ... Lewin, J. S. (1998). Brain activation during silent word generation evaluated with functional MRI. *Brain and Language*, *64*, 231–256.
- Giraud, A. L., Kell, C., Thierfelder, C., Sterzer, P., Russ, M. O., Preibisch, C., & Kleinschmidt, A. (2004). Contributions of sensory input, auditory search and verbal comprehension to cortical activity during speech processing. *Cerebral Cortex*, *14*, 247–255.
- Glasser, M. F., Sotiropoulos, S. N., Wilson, J. A., Coalson, T. S., Fischl, B., Andersson, J. L., ... Jenkinson, M. (2013). The minimal preprocessing pipelines for the Human Connectome Project. *Neuroimage*, *80*, 105–124.
- Goel, V., Gold, B., Kapur, S., & Houle, S. (1998). Neuroanatomical correlates of human reasoning. *Journal of Cognitive Neuroscience*, *10*, 293–302.
- Gusnard, D., Akbudak, E., Shulman, G., & Raichle, M. E. (2001a). Role of medial prefrontal cortex in a default mode of brain function. *NeuroImage*, *13*, S414–S414.
- Gusnard, D. A., Akbudak, E., Shulman, G. L., & Raichle, M. E. (2001b). Medial prefrontal cortex and self-referential mental activity: Relation to a default mode of brain function. *Proceedings of the National Academy of Sciences of the United States of America*, *98*, 4259–4264.
- Gutierrez-Sigut, E., Payne, H., & MacSweeney, M. (2015). Investigating language lateralization during phonological and semantic fluency tasks using functional transcranial Doppler sonography. *Laterality*, *20*, 49–68.
- Hesling, I., Clement, S., Bordesoules, M., & Allard, M. (2005). Cerebral mechanisms of prosodic integration: Evidence from connected speech. *NeuroImage*, *24*, 937–947.
- Iacoboni, M., Molnar-Szakacs, I., Gallese, V., Buccino, G., Mazziotta, J. C., & Rizzolatti, G. (2005). Grasping the intentions of others with one's own mirror neuron system. *PLoS Biology*, *3*, 529–535.
- Jastorff, J., Clavagner, S., Gergely, G., & Orban, G. A. (2011). Neural mechanisms of understanding rational actions: Middle temporal Gyrus activation by contextual violation. *Cerebral Cortex*, *21*, 318–329.
- Ji, B., Li, Z. H., Li, K. M., Li, L. C., Langley, J., Shen, H., ... Hu, X. P. (2016). Dynamic thalamus parcellation from resting-state fMRI data. *Human Brain Mapping*, *37*, 954–967.
- Brodmann, K. (1909). *Vergleichende Lokalisationslehre der Grobhirnrinde in ihren Prinzipien dargestellt auf Grund des Zellenbaues*. Leipzig, Germany: Barth.
- Kahnt, T., Chang, L. J., Park, S. Q., Heinzle, J., & Haynes, J. D. (2012). Connectivity-based parcellation of the human orbitofrontal cortex. *The Journal of Neuroscience*, *32*, 6240–6250.
- Kelly, C., Toro, R., Di Martino, A., Cox, C. L., Bellec, P., Castellanos, F. X., & Milham, M. P. (2012). A convergent functional architecture of the insula emerges across imaging modalities. *NeuroImage*, *61*, 1129–1142.
- Kilner, J. M. (2011). More than one pathway to action understanding. *Trends in Cognitive Sciences*, *15*, 352–357.
- Kim, J. H., Lee, J. M., Jo, H. J., Kim, S. H., Lee, J. H., Kim, S. T., ... Saad, Z. S. (2010). Defining functional SMA and pre-SMA subregions in human MFC using resting state fMRI: Functional connectivity-based parcellation method. *NeuroImage*, *49*, 2375–2386.
- Kim, J. J., Crespo-Facorro, B., Andreasen, N. C., O'Leary, D. S., Zhang, B., Harris, G., & Magnotta, V. A. (2000). An MRI-based parcellation method for the temporal lobe. *NeuroImage*, *11*, 271–288.
- Knecht, S., Deppe, M., Drager, B., Bobe, L., Lohmann, H., Ringelstein, E. B., & Henningsen, H. (2000). Language lateralization in healthy right-handers. *Brain*, *123*, 74–81.
- Koster-Hale, J., & Saxe, R. (2013). Theory of mind: A neural prediction problem. *Neuron*, *79*, 836–848.
- Li, H., Fan, L., Zhuo, J., Wang, J., Zhang, Y., Yang, Z., & Jiang, T. (2017). ATPP: A pipeline for automatic Tractography-based brain Parcellation. *Frontiers in Neuroinformatics*, *11*, 35.
- Liu, C. H., Tang, L. R., Gao, Y., Zhang, G. Z., Li, B., Li, M., ... Wang, L. (2019). Resting-state mapping of neural signatures of vulnerability to depression relapse. *Journal of Affective Disorders*, *250*, 371–379.
- McDermott, K. B., Petersen, S. E., Watson, J. M., & Ojemann, J. G. (2003). A procedure for identifying regions preferentially activated by attention to semantic and phonological relations using functional magnetic resonance imaging. *Neuropsychologia*, *41*, 293–303.
- Mirz, F., Ovesen, T., Ishizu, K., Johannsen, P., Madsen, S., Gjedde, A., & Pedersen, C. B. (1999). Stimulus-dependent central processing of auditory stimuli—A PET study. *Scandinavian Audiology*, *28*, 161–169.
- Mishra, A., Rogers, B. P., Chen, L. M., & Gore, J. C. (2014). Functional connectivity-based Parcellation of amygdala using self-organized mapping: A data driven approach. *Human Brain Mapping*, *35*, 1247–1260.
- Molenberghs, P., Trautwein, F. M., Bockler, A., Singer, T., & Kanske, P. (2016). Neural correlates of metacognitive ability and of feeling confident: A large-scale fMRI study. *Social Cognitive and Affective Neuroscience*, *11*, 1942–1951.
- Nebel, M. B., Joel, S. E., Muschelli, J., Barber, A. D., Caffo, B. S., Pekar, J. J., & Mostofsky, S. H. (2014). Disruption of functional organization within the primary motor cortex in children with autism. *Human Brain Mapping*, *35*, 567–580.
- Nelson, S. M., Cohen, A. L., Power, J. D., Wig, G. S., Miezin, F. M., Wheeler, M. E., ... Petersen, S. E. (2010). A Parcellation scheme for human left lateral parietal cortex. *Neuron*, *67*, 156–170.
- Nelson, S. M., Dosenbach, N. U. F., Cohen, A. L., Wheeler, M. E., Schlaggar, B. L., & Petersen, S. E. (2010). Role of the anterior insula in task-level control and focal attention. *Brain Structure & Function*, *214*, 669–680.
- Ogawa, R., Kagitani-Shimono, K., Matsuzaki, J., Tanigawa, J., Hanaie, R., Yamamoto, T., ... Taniike, M. (2019). Abnormal cortical activation during silent reading in adolescents with autism spectrum disorder. *Brain & Development*, *41*, 234–244.
- Rademacher, J., Galaburda, A. M., Kennedy, D. N., Filipek, P. A., & Caviness, V. S., Jr. (1992). Human cerebral cortex: Localization, parcellation, and morphometry with magnetic resonance imaging. *Journal of Cognitive Neuroscience*, *4*, 352–374.
- Raichle, M. E., MacLeod, A. M., Snyder, A. Z., Powers, W. J., Gusnard, D. A., & Shulman, G. L. (2001). A default mode of brain function. *Proceedings of the National Academy of Sciences of the United States of America*, *98*, 676–682.
- Rizzolatti, G., Fadiga, L., Matelli, M., Bettinardi, V., Paulesu, E., Perani, D., & Fazio, F. (1996). Localization of grasp representations in humans by PET: 1. Observation versus execution. *Experimental Brain Research*, *111*, 246–252.
- Sato, W., Toichi, M., Uono, S., & Kochiyama, T. (2012). Impaired social brain network for processing dynamic facial expressions in autism spectrum disorders. *BMC Neuroscience*, *13*, 99.
- Schubotz, R. I., Wurm, M. F., Wittmann, M. K., & von Cramon, D. Y. (2014). Objects tell us what action we can expect: Dissociating brain areas for retrieval and exploitation of action knowledge during action observation in fMRI. *Frontiers in Psychology*, *5*, 636.
- Schurz, M., Radua, J., Aichhorn, M., Richlan, F., & Perner, J. (2014). Fractionating theory of mind: A meta-analysis of functional brain imaging studies. *Neuroscience and Biobehavioral Reviews*, *42*, 9–34.
- Schurz, M., Tholen, M. G., Perner, J., Mars, R. B., & Sallet, J. (2017). Specifying the brain anatomy underlying temporo-parietal junction activations for theory of mind: A review using probabilistic atlases from different imaging modalities. *Human Brain Mapping*, *38*, 4788–4805.
- Sewards, T. V. (2011). Adolf Hopf's 1954 myeloarchitectonic parcellation of the human temporal lobe: A review and assessment. *Brain Research Bulletin*, *86*, 298–313.

- Smith, S. M., Fox, P. T., Miller, K. L., Glahn, D. C., Fox, P. M., Mackay, C. E., ... Beckmann, C. F. (2009). Correspondence of the brain's functional architecture during activation and rest. *Proceedings of the National Academy of Sciences of the United States of America*, *106*, 13040–13045.
- Tench, C. R., Tanasescu, R., Auer, D. P., Cottam, W. J., & Constantinescu, C. S. (2014). Coordinate based meta-analysis of functional neuroimaging data using activation likelihood estimation; full width half max and group comparisons. *Plos One*, *9*, 9.
- Tian, F., Diao, W., Yang, X., Wang, X., Roberts, N., Feng, C., & Jia, Z. (2019). Failure of activation of striatum during the performance of executive function tasks in adult patients with bipolar disorder. *Psychological Medicine*, 1–13. <https://doi.org/10.1017/S0033291719000473>. [Epub ahead of print]
- Valyear, K. F., & Culham, J. C. (2010). Observing learned object-specific functional grasps preferentially activates the ventral stream. *Journal of Cognitive Neuroscience*, *22*, 970–984.
- Vincent, J. L., Patel, G. H., Fox, M. D., Snyder, A. Z., Baker, J. T., Van Essen, D. C., ... Raichle, M. E. (2007). Intrinsic functional architecture in the anaesthetized monkey brain. *Nature*, *447*, 83–86.
- Vingerhoets, G., & Stroobant, N. (1999). Lateralization of cerebral blood flow velocity changes during cognitive tasks--A simultaneous bilateral transcranial Doppler study. *Stroke*, *30*, 2152–2158.
- Wang, J., Becker, B., Wang, L., Li, H., Zhao, X., & Jiang, T. (2019). Corresponding anatomical and coactivation architecture of the human precuneus showing similar connectivity patterns with macaques. *NeuroImage*, *200*, 562–574.
- Wang, J., Fan, L., Wang, Y., Xu, W., Jiang, T., Fox, P. T., ... Jiang, T. (2015). Determination of the posterior boundary of Wernicke's area based on multimodal connectivity profiles. *Human Brain Mapping*, *36*, 1908–1924.
- Wang, J., Fan, L., Zhang, Y., Liu, Y., Jiang, D., Zhang, Y., ... Jiang, T. (2012). Tractography-based parcellation of the human left inferior parietal lobule. *NeuroImage*, *63*, 641–652.
- Wang, J., Xie, S., Guo, X., Becker, B., Fox, P. T., Eickhoff, S. B., & Jiang, T. (2017). Correspondent functional topography of the human left inferior parietal lobule at rest and under task revealed using resting-state fMRI and Coactivation based Parcellation. *Human Brain Mapping*, *38*, 1659–1675.
- Wang, J., Yang, Y., Fan, L., Xu, J., Li, C., Liu, Y., ... Jiang, T. (2015). Convergent functional architecture of the superior parietal lobule unraveled with multimodal neuroimaging approaches. *Human Brain Mapping*, *36*, 238–257.
- Wang, J., Zhang, J., Rong, M., Wei, X., Zheng, D., Fox, P. T., ... Jiang, T. (2016). Functional topography of the right inferior parietal lobule structured by anatomical connectivity profiles. *Human Brain Mapping*, *37*, 4316–4332.
- Wang, J., Zuo, Z., Xie, S., Miao, Y., Ma, Y., Zhao, X., & Jiang, T. (2018). Parcellation of macaque cortex with anatomical connectivity profiles. *Brain Topography*, *31*, 161–173.
- Wheatley, B. M. (2008). Selective amygdalohippocampectomy: The trans-middle temporal gyrus approach. *Neurosurgical Focus*, *25*, E4.
- Whitney, C., Jefferies, E., & Kircher, T. (2011). Heterogeneity of the left temporal lobe in semantic representation and control: Priming multiple versus single meanings of ambiguous words. *Cerebral Cortex*, *21*, 831–844.
- Wig, G. S., Schlaggar, B. L., & Petersen, S. E. (2011). Concepts and principles in the analysis of brain networks. *Annals of the New York Academy of Sciences*, *1224*, 126–146.
- Wirth, M., Jann, K., Dierks, T., Federspiel, A., Wiest, R., & Horn, H. (2011). Semantic memory involvement in the default mode network: A functional neuroimaging study using independent component analysis. *NeuroImage*, *54*, 3057–3066.
- Xu, J., Wang, J., Fan, L., Li, H., Zhang, W., Hu, Q., & Jiang, T. (2015). Tractography-based Parcellation of the human middle temporal Gyrus. *Scientific Reports*, *5*, 18883.
- Yates, S. L., Barach, A., Gingell, S., Whalley, H. C., Job, D., Johnstone, E. C., ... Lawrie, S. M. (2006). Parcellating the temporal lobes from magnetic resonance images using generic software in subjects at high risk of developing schizophrenia. *Psychiatry Research: Neuroimaging*, *147*, 197–212.

SUPPORTING INFORMATION

Additional supporting information may be found online in the Supporting Information section at the end of this article.

How to cite this article: Xu J, Lyu H, Li T, et al. Delineating functional segregations of the human middle temporal gyrus with resting-state functional connectivity and coactivation patterns. *Hum Brain Mapp*. 2019;40:5159–5171. <https://doi.org/10.1002/hbm.24763>